PCCP

UV/Vis/near-IR spectroscopic characteristics of $H_{4-x}Cs_xPVMo_{11}O_{40}$ ($x = 0, 2$) catalyst under different temperatures and gas atmospheres

J. Melsheimer,*[a] J. Kröhnert,[a] R. Ahmad,[a] S. Klokishner,[b] F. C. Jentoft,[a] G. Mestl[a] and R. Schlögl[a]

[a] *Fritz-Haber-Institut der Max-Planck-Gesellschaft, Department of Inorganic Chemistry, Faradayweg 4-6, D-14195 Berlin, Germany. E-mail: jm@FHI-Berlin.mpg.de*
[b] *State University of Moldova, Mateevich str.60, 2009 Kishinev, Moldova. E-mail: sophia@usm.md*

Received 11th October 2001, Accepted 8th March 2002
First published as an Advance Article on the web 29th April 2002

In order to understand the transformations of the Keggin-type $H_{4-x}Cs_xPV{-}Mo_{11}O_{40}$ ($x = 0, 2$) compounds with rising temperature over a long time in a stream of different gas atmospheres, *in situ* UV/Vis/near-IR spectroscopic studies were carried out. Diffuse reflectance spectra were recorded using an improved spectrometer and a suitable microreactor. Visible and near-IR peak intensities, peak positions and the band gap energies were determined from apparent absorption spectra. Propene, isopropanol, water and the oxidation products were analyzed by GC. The experimentally observed blue shift of the visible absorption band in the region of crystal water loss and the increase in the near-IR absorption were explained on the basis of quantum-mechanical calculations of the shapes and positions of the charge transfer and d–d bands arising from Mo^{5+}–Mo^{6+} and V^{4+}–Mo^{6+} pairs in intact and ill-defined fragments of the Keggin structure. It was concluded that with removal of crystal water during the action of He, He/H_2O, propene, O_2/propene and increasing temperature, reduced species with protons located at the bridging oxygens promote a blue shift of the visible band, while a large number of ill-defined species form the near-IR part of the spectra in the temperature range 326–600 K.

1. Introduction

Cs salts of vanadiummolybdophosphoric acid, used because of their good redox and acid/base properties, are, for example, catalyst precursors for the oxidative dehydrogenation reaction of isobutyric acid to methacrylic acid.[1–3] Unfortunately, however, the title compound, in particular with $x = 0$, is thermally unstable, which makes it especially difficult to determine the catalytically active center. Many efforts have been made to investigate the thermally unstable state, for example, by XRD,[2,4] TG-DTA coupled with IMR-MS and DSC,[2,5] IR,[4,6–8] EPR[9,10] and Raman.[11–13] To improve the stability and catalytic activity of such compounds, cations were introduced in the secondary structure.[14,15] Recently, the caesium-containing compound with $x = 2$ proved to be the best catalyst among the different title compounds, for instance for the partial oxidation of ethene and propene by molecular oxygen.[14–16] An important role in the structural dynamics of this type of compound is played by the reducibility of the cationic centres, which was investigated by EPR spectroscopy.[10] Changes in the redox state of heteropoly compounds can also be investigated by the UV/Vis/near-IR spectroscopy. In the case of gas/solid reactions this method is restricted to the reflectance mode because the absorption in the catalyst samples, which must have a certain necessary thickness, is too high. During changes in the redox state the spectroscopic characteristics, such as the number of the absorption bands, peak positions and band gap energies, also change. Besides the oxygen ligand to metal charge transfer band (LMCT) there are absorption bands which can develop or disappear due to the optical d–d transitions in V^{4+} and Mo^{5+} and intervalence V^{4+}–Mo^{6+} and/or Mo^{5+}–Mo^{6+} optical transitions. Up to now, this spectroscopic method has been applied to the investigation of heteropoly compounds by some groups, but all spectra were recorded *ex situ*.[17–21] The heteropoly compounds alter the spectroscopic behaviour due to the loss of water.[22,23] In certain compounds of this type, even a small water loss leads to noticeable changes in the absorption band intensity. The resulting strong alterations of light absorption can only be observed with improved spectroscopic equipment.[24] We report here on a systematic *in situ* study of the influence of both an inert gas (He) and other gas atmospheres (O_2, propene, O_2/propene) on the spectroscopic feature at room temperature and higher temperatures, respectively. The goal of the paper is also to find a correlation between the spectroscopic characteristics and catalytic data for the oxidation of propene on the title compounds.

In ref. 25 a model was worked out for the calculation of the charge transfer and d–d bands arising from the homonuclear Mo^{5+}–Mo^{6+} and heteronuclear V^{4+}–Mo^{6+} pairs in intact and ill-defined fragments of the Keggin structure contributing to the absorption spectra under different experimental conditions. Electron transfer processes $V^{4+}\text{–O–}Mo^{6+} \rightarrow V^{5+}\text{–O–}Mo^{5+}$, $Mo^{5+}\text{–O–}Mo^{6+} \rightarrow Mo^{6+}\text{–O–}Mo^{5+}$ involving two metal centers were taken into consideration. The vibronic coupling constants and crystal field splittings determining the positions and the shapes of the charge transfer and d–d bands were calculated in the exchange charge model[26] of the crystal field. In the present paper, on the basis of the regularities established in ref. 25, a qualitative explanation of the temperature behaviour of the visible (Vis) and near-IR (NIR) parts of the absorption spectra of $H_{4-x}Cs_x PVMo_{11}O_{40}$ ($x = 0,2$) will be given. Along with this, the band gap energies that change with different gas atmospheres will be determined as a function of temperature.

DOI: 10.1039/b109293f

2. Experimental

A Perkin-Elmer Lambda 9 spectrometer with an enlarged integrating sphere and a flow-through microreactor was used for *in situ* UV/Vis/NIR diffuse reflectance spectroscopy on different dilute catalyst samples up to 663 K. In the home-made flow-through microreactor, temperature gradients in the catalyst bed of up to 30 K were registered at the highest temperatures. Approximately 110 mg of the catalyst were mixed with SiO_2 (Heraeus, 0.1–0.4 mm) (7–10 wt.%) and placed in a home-made microreactor operating under continuous gas flow. All spectroscopic measurements were carried out sequentially with a scan speed of 240 nm min^{-1}, a slit width of 5.0 nm and a response time of 0.5 s, as well as with a spectralon as a reference.

The free heteropoly acid ($H_4PVMo_{11}O_{40}$), denoted as HPA, was prepared by hydrothermal synthesis from a stoichiometric mixture of metal oxides (MoO_3, V_2O_5) and phosphoric acid in water. Cs_2CO_3 and the solution of heteropoly acid were used for the preparation of the Cs_2 salt ($Cs_2H_2PVMo_{11}O_{40}$), denoted as Cs_2A.

The gases used were helium (purity > 99.999 vol.%), helium saturated with water at room temperature (RT) and oxygen (purity > 99.998 vol.%). In addition, the feed mixture was 10 vol% propene (purity $\geqslant$ 99.8 vol.%) in helium or 10 vol% propene plus 10 vol% oxygen in helium with a total gas flow of 71 or 74 ml min^{-1}, respectively. Oxygen, propene and the reaction products were analyzed on-line with two gas chromatographs (Perkin Elmer), equipped with heated automatic gas sampling valves, an FFAP column (Macherey-Nagel) and a packed Carboxen-1000 column using an FID and a TCD.

Three different methods of gas atmosphere treatment were applied for spectra recording. First, He treatment was carried out for about 12 h at RT. Second, propene/He treatment was carried out for about 2 h at RT, and then the temperature was increased at a rate of 1 K min^{-1} to 323 K, and the spectra were recorded over a period of *ca.* 5 h. Third, an isochronic–isothermic temperature–time program was chosen for all gas atmospheres as follows: gas atmosphere treatment for *ca.* 2 h at RT, whereby RT_1 denotes the initial spectrum and RT_2 the spectrum after 2 h on gas flow. Then the temperature was increased from RT_2 to 326 K with a heating rate of 1 K min^{-1} and from this temperature to 663 K in steps of ~50 K at the same heating rate, with a holding time of 2 h for each gas at each temperature.

For all operations described in sections 3 and 4, the last spectrum was always taken before the temperature was increased. The holding time of 2 h was sufficient because no spectroscopic changes were observed after this time. The apparent absorption was evaluated from the diffuse reflectance data using the formula $1 - R_{mixture}/R_{SiO_2}$, whereby at each desired temperature the measured reflectance data of the mixture were divided by the pure SiO_2 diluent. For some spectra it was necessary to eliminate the jumps close to the lamp (*ca.* 320 nm) and the detector change (*ca.* 860 nm). In addition, the reflectance data in short wavelength ranges near these particular points were smoothed.

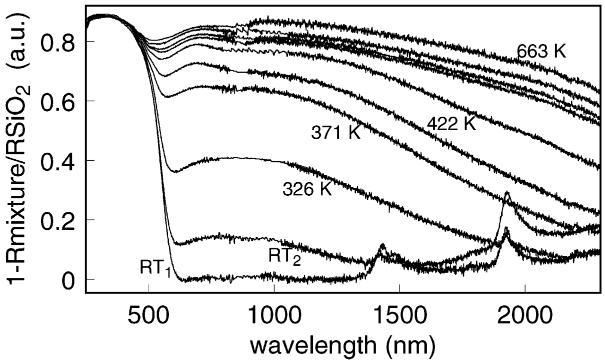

Fig. 1 Spectroscopic screening for He/$H_2Cs_2PVMo_{11}O_{40}$ from RT to 663 K. RT_1 : RT, He flux : 6 min; RT_2 : RT, He flux 105 min.

3. Determination of spectroscopic characteristics

From Fig. 1 it is seen that above 326 K, the intensity of the spectra increases significantly both in the Vis and near-IR range. The investigation with Raman spectroscopy[13] shows that the formation of ill-defined clusters takes place at higher temperatures. Therefore the transformations of the spectrain the range $326 < T < 663$ K are attributed to these clusters. Correspondingly, the spectral intensities were determined by integration in the range of $A < \lambda < B$, where A is the lowest point of the band edge and B is 2000 nm. The upper limit of this interval was determined in correspondence with the results obtained in ref. 25 which showed that the maximum of the lower energy intervalence charge transfer band arising from ill-defined dimeric clusters is about 2000 nm. For fixed temperatures the relative spectrum intensity was determined as $n = I_i/I_0$ where I_i and I_0 are the intensities of spectra at temperatures T and $T = 663$ K. The peak positions of the absorption bands were evaluated after a linear background subtraction. The spectra of heteropoly compounds in the range of light-induced LMCT are usually interpreted as interband optical transitions or transitions between discrete molecular orbitals. However, we employ the band model bearing in mind two factors: Firstly, the disintegration of heteropoly compounds examined is accompanied by water removal (crystal or constitutional water). Independent of the stage of disintegration of the Keggin units, the mean geometric distance between them decreases. This facilitates polymerisation and thus interunit electron transfer. Secondly, the final product of disintegration is the semiconductor MoO_3. The filled valence band and the conduction band are formed by the oxygen 2p and metal d orbitals,[27] respectively. At the beginning of the experiment (RT_1, short time on gas flux), when the intervalent charge transfer (IVCT) and d–d bands are not yet developed, the absorption band edge is determined as a point at which the slope of the apparent absorption coefficient for the LMCT band is at its maximum. At higher temperatures in the range of 400–600 nm the overlap of the LMCT band, d–d and IVCT bands becomes appreciable, and this procedure does not lead to reasonable results. Therefore, for temperatures above RT_1 we evaluate the shift of the absorption band edge relative to its position under the initial experimental conditions. Assuming that for direct interband optical transitions the apparent absorption coefficient is a function f of $\hbar\omega - E_g$ (where $\hbar\omega$ is the photon energy, and E_g is the optical band gap energy) at different temperatures we estimate the values $\hbar\omega$ corresponding to a fixed value of f equal to f_0 and taken in the vicinity of the maximum of the LMCT band, *i.e.*, in the range within which the UV absorption is not affected by the d–d and IVCT transitions. The change $\hbar\Delta\omega$ in the photon energy determined in this way is equal to the shift ΔE_g of the absorption band edge.

4. Results and discussion

4.1. Peak intensity *versus* time on He stream at room temperature

The loss of crystal water can be observed from the change in the near-IR absorption bands at 1430 and 1930 nm. Such a water loss, recognizable in the decreasing peak intensity, is already observed at RT in dependence upon time on He stream, as can be seen in Fig. 2. In addition, in the ultraviolet spectral range HPA and Cs_2A exhibit pronounced LMCT

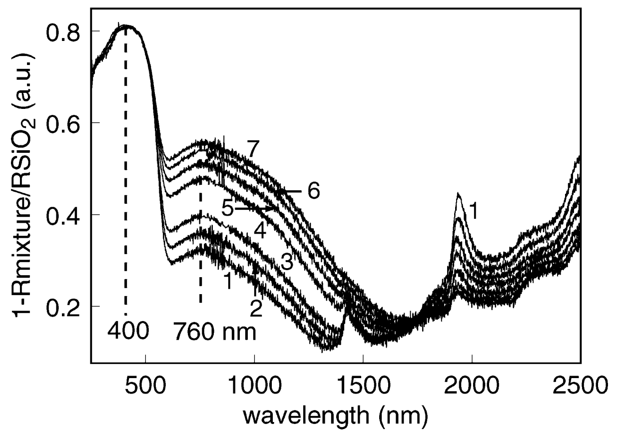

Fig. 2 Experimental UV/Vis/near-IR diffuse reflectance spectra of $H_4PVMo_{11}O_{40}$ in dependence upon time on He stream at room temperature. Time on stream (h) : 1.4 (1); 1.9 (2); 2.4 (3); 9.9 (6); 12.3 (7).

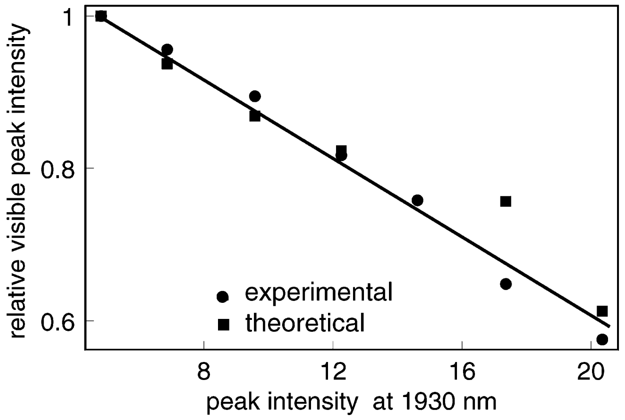

Fig. 3 Relative visible peak intensity of $He/H_4PVMo_{11}O_{40}$ at room temperature calculated from experimental and theoretical spectra *vs.* peak intensity at 1930 nm.

bands at *ca.* 400 and 360 nm,respectively. The intensity and the shape of this band do not change during the action of the He stream. In the Vis/near-IR range an asymmetrical broad band is observed, whose peak intensity increases with increasing time on He stream. The peak maximum of this band is located in the range 740–780 nm and a shoulder can be distinguished in the range 900–1000 nm. A semiempirical model that considers a dimeric cluster V^{4+}–Mo^{6+} was employed for the simulation of the spectra.[28] At 300 K under He the spectra of HPA in the Vis/near-IR range were shown to be determined by the optical d–d transitions in V^{4+} and Mo^{5+} ions with intact oxygen surroundings (MO_6) and the intervalence transition V^{4+}–Mo^{6+}. The maximum observed in the range 740–780 nm (Fig. 2) was assigned to the intense b_2–e (d–d) transitions in V^{4+} and Mo^{5+}. The shoulder in the range 900–1000 nm was assigned to an IVCT peak of the heteronuclear pair V–Mo. Appreciable spectroscopic changes between 600 and 1300 nm were attributed to the increase in the parameter characterising electron transfer between the V^{4+} and Mo^{6+} ions (electron transfer parameter) due to water loss. By varying this parameter a good fit of the calculated spectra to the experimental ones could be obtained.[28] Besides the electron transfer parameter all other characteristic system parameters were determined from experimental data. The theoretical calculations[28] make it possible to separate the contributions of the d–d transitions and the charge transfer band from the total spectrum intensity. At RT the relative contribution of the d–d transitions decreases appreciably with time on He stream, while the intensity of the charge transfer band grows with the increase in the transfer parameter. For example, for the spectrum recorded at RT after 12.2 h on He stream these contributions are 34% (d–d) and 66% (charge transfer). In addition, it was determined that the peak intensity of the near-IR H_2O absorption bands correlates with the peak intensity in the range indicated above. Fig. 3 shows this connection for HPA treated in He selecting the greater near-IR H_2O peak intensity at 1930 nm.

4.2. Spectroscopic screening in dependence upon the gas atmosphere and temperature

For Cs_2A treated in He from RT to 663 K the apparent absorption increases strongly with the temperature (Fig. 1). Such an increase in UV/Vis was already shown and discussed in ref. 22. Simultaneously, the near-IR absorption bands of the crystal water disappear completely, with the consequence that a Vis broad absorption band, and at higher temperatures additionally a near-IR absorption band, can be clearly detected. A similar feature is observed for HPA in the presence of He. In contrast, the spectroscopic feature for HPA and Cs_2A is different in the presence of propene or the mixture of O_2/propene instead of He. After a time on stream of 2 h the apparent absorption already increases enormously at RT in the presence of propene. No water band could be detected any longer in the presence of propene for Cs_2A after this time at RT and for HPA after 2 h at 326 K (not shown). The reason for the very strong increase in the apparent absorption in the presence of propene is that propene apparently draws the crystal water from the catalyst, and when that has disappeared the constitutional water as well. The Vis peak position suffers a blue shift from 740 nm to 700 nm after a time on stream of *ca.* 90 min with a slight temperature increase (to 319 K) (not shown), accompanied by the formation of isopropanol detected by GC. In the presence of O_2 the increase in the apparent absorption is not as strong as in the case of He and the removal of water molecules proceeds more slowly with increasing time on stream and temperature. In addition, for HPA treated in O_2 no successive increase in the apparent absorption is observed with increasing temperature, so that, for instance, the apparent absorption in a certain temperature range can be greater than at higher temperatures. He saturated with water appears to have a stabilizing action on these compounds. The water bands disappear only at 473 K (not shown).

4.3. Influence of gas atmospheres on the visible and near-IR peak intensity between RT and 663 K

With the exception of He/H_2O, the Vis and near-IR peak intensities increase strongly in the presence of the gas atmospheres applied up to 371 K, as can be seen in Table 1. The initial dramatic change in the Vis and near-IR peak intensity points to the crystal water loss which already begins at RT (see section 4.1) and continues up to 400–420 K. A lower change in peak intensity is observed in the range 520–540 K (Table 1), wherein the constitutional water loss begins.[14,15]

As already mentioned in section 4.2., the strongest increase can be recognized for both catalysts in the presence of propene and the mixture of O_2/propene up to 371 K. In contrast, the peak intensity decreases rapidly for HPA in the presence of O_2 above 371 K, and above 467 K no peak intensity was observed. For Cs_2A the peak intensity increases in the presence of O_2 similarly to the increase in the presence of He. However, the peak intensity is higher than that of He in the range 326–608 K. Another peak intensity *vs.* temperature curve is observed in the presence of He/H_2O. A clear increase in this intensity can only be detected above 371 K.

For HPA the decrease in the peak intensity of the Vis and near-IR absorption band above 371 K (Table 1) in the presence of O_2 may be attributed to the oxidation of Mo^{5+} and V^{4+} centers by this gas phase. For HPA the O_2 produces such

Table 1 Influence of gas atmospheres and temperature on the relative Vis and near-IR peak intensities and TG of $H_{4-x}Cs_xPVMo_{11}O_{40}$ ($x = 0, 2$). TG data recorded under He (50 ml min^{-1}) with 5 K min^{-1}

	Relative Vis and near-IR peak intensity					
Temperature/K	He	He/H_2O	Propene	O_2	O_2/propene	TG weight loss of water (%)
$H_4PVMo_{11}O_{40}$						
RT_1	0.1212	0.0111	0.0468	0.0107	0.2291	0
RT_2	0.1180	0.1480	0.4732	0.0117	0.4609	0.26
325.9	0.2873	0.1284	0.6291	0.4009	0.7523	0.69
371.3	0.7106	0.2328	0.7323	1.0	0.7951	4.90
422.1	0.8126	0.6569	0.7115	0.4960	0.7396	10.40
466.8	0.8865	0.9082	0.8133	0.2491	0.6925	10.90
511.5	0.8991	0.9412	0.8533	—	0.7459	11.00
561.1	0.8517	0.9679	0.8514	—	0.7805	11.30
607.5	0.9237	0.9981	0.9926	—	0.8430	12.00
663.1	1.0	1.0	1.0	—	1.0	12.60
$Cs_2H_2PVMo_{11}O_{40}$						
RT_1	0.0088	0.0445	0.6159	0.0230	0.0088	0
RT_2	0.0724	0.0766	—	0.1521	0.8119	0.15
325.9	0.3219	0.0864	0.8325	0.4311	0.8438	0.38
371.3	0.6148	0.1297	0.8773	0.5133	0.9056	2.00
422.1	0.7132	0.7223	0.9309	0.6119	0.8329	2.70
466.8	0.8420	0.8364	0.9447	0.7358	0.8429	2.87
511.5	0.9120	0.8711	0.9614	0.8682	0.8799	3.05
561.1	0.9316	0.8954	0.9737	0.9537	0.9243	3.27
607.5	0.9595	0.9417	0.9855	0.9813	0.9671	3.45
663.1	1.0	1.0	1.0	1.0	1.0	3.45

a strong oxidation that no more absorption bands could be identified. In contrast, the Cs^+ ions play a stabilizing role in the Cs_2A salt and hinder significant oxidation. Above 512 K, for HPA and Cs_2A the Vis and near-IR peak intensity increase under reaction conditions (O_2/propene).

4.4. Influence of gas atmospheres on the visible peak position between RT and 663 K

Table 2 shows that the peak position of the Vis absorption band is blue shifted for HPA in the presence of He, the mixture of O_2/propene, or propene (strong shift) with increasing temperature. For Cs_2A in the presence of these gas atmospheres, the spectroscopic feature is the same up to 371 K (propene), 422 K (He) and *ca.* 467 K (O_2/propene), as can be seen in Table 2. Above these temperatures the Vis peak positions are nearly constant (He, propene) or increase slightly (O_2/propene). In contrast, a Vis peak position for HPA treated in O_2 can only be observed up to 371 K, and for Cs_2A treated in the same gas an increase is detected after a decrease up to 371 K. In the case of O_2/Cs_2A two data sets show the same spectroscopic trend (Table 2). He/H_2O appears to have a stabilizing effect up to *ca.* 371 K and 422 K for HPA and Cs_2A, respectively (Table 2). If the crystal water is removed with increasing temperature one observes a blue shift of the Vis peak position that is lower in the case of Cs_2A than of HPA. However, such a shift is not detected for Cs_2A with the exception of He/H_2O and O_2 in the temperature range in which the constitutional water is removed (Table 2).

The results obtained can be explained on the basis of calculations carried out in ref. 25. For a clearer understanding of the interpretation presented below we first give a short description of the background of the model employed.[25] We consider a reduced Keggin unit. Depending upon time on gas flux and temperature the nearest oxygen surrounding of the i-th ($i = 1$–12) metal ion (M) in the Keggin unit may be unimpaired (MO_6) or ill-defined ($M((O_t)_{1-s_i}(O_p)_{1-y_i}(O_b)_{4-x_i}\ H_{\alpha z_i})$), where O_b, O_t are the bridging and terminal oxygens, O_p stands for the oxygen in a phosphorus tetrahedral environment, s_i, x_i and y_i are the numbers of oxygen ions extracted in the process of constitutional water or oxygen evolution, z_i is the number of protons localized on the moiety, $\alpha = $ b or t for protons residing on the oxygens O_b and O_t, respectively. As in the Piepho–Krausz–Schatz model[29] the extra electron localized on a certain site (metal ion) is supposed to interact with the full symmetric displacement ("breathing" mode) of the local surrounding. The full-symmetric dimensionless coordinates for the twelve ($M((O_t)_{1-s_i}\ (O_p)_{1-y_i}(O_b)_{4-x_i}H_{\alpha z_i})$) units will be denoted as q_i ($i = 1$–12). The full Hamiltonian of the system can be presented as

$$H = H_e + H_v + H_{ev}, \qquad (1)$$

where H_e is the electronic Hamiltonian determining the wave functions and the eigenvalues of a Keggin molecule in the fixed nuclear configuration ($q_i = 0$), H_L is the Hamiltonian of free lattice vibrations, and H_{ev} is the vibronic interaction Hamiltonian. The electronic Hamiltonian H_e includes two parts:

$$H_e = h_0 + g, \qquad (2)$$

where the one electronic operator h_0 involves the kinetic and potential energies of all d-electrons, g is the two-particle (interelectronic) repulsion. The free harmonic vibrations (with the frequencies ω) of the twelve $M((O_t)_{1-s_i}(O_p)_{1-y_i}(O_b)_{4-x_i}\ H_{\alpha z_i})$ units are assumed to be vibronically independent, and the Hamiltonian H_v has the form:

$$H_v = \frac{\hbar\omega}{2}\sum_{i=1}^{12}\left(q_i^2 - \frac{\partial^2}{\partial q_i^2}\right) \qquad (1)$$

The vibronic interaction Hamiltonian in our model is supposed to be linear with respect to the atomic displacements

Table 2 Vis peak positions of $H_{4-x}Cs_xPVMo_{11}O_{40}$ ($x = 0$, 2) in dependence on some gas atmospheres and temperature

	Vis peak position/nm				
Temperature /K	He	He/H_2O	Propene	O_2	O_2/propene
$H_4PVMo_{11}O_{40}$					
RT_1	740	773	737	740	742
RT_2	750	765	737	750	748
325.9	739	788	743	761	738
371.3	731	770	691	747	737
422.1	740	766	689	—	733
466.8	715	750	660	—	711
511.5	698	729	665	—	704
561.1	680	694	641	—	697
607.5	670	669	636	—	679
663.1	668	677	644	—	—
$Cs_2H_2PVMo_{11}O_{40}$					
RT_1	760	750	770	727.5 ± 2.5	752
RT_2	771	750	717	748 ± 8	—
325.9	748	740	695	751 ± 3	730
371.3	724	740	685	730.5 ± 0.5	716
422.1	710	742	687	734 ± 0	709
466.8	709	736	695	752.5 ± 2	705
511.5	711	733	693	754 ± 3	710
561.1	710	732	692	750.5 ± 3	718
607.5	712	732	—	749 ± 6	718
663.1	709	714	—	742 ± 4	726

and can be represented in the following form:

$$H_{\mathrm{ev}} = \sum_k \sum_i v_i(\vec{r}_k) q_i \tag{4}$$

where the functions $v_i(\vec{r}_k)$ of the electronic coordinates $\vec{r}_k$ are determined as the derivatives of the electron-nuclear potential energy $W(|\vec{r}_k - \vec{R}_{i\alpha}|)$ in the points $q_i = 0$:

$$\begin{aligned} v_i(\vec{r}_k) &= \sum_\alpha \left(\frac{\partial W(|\vec{r}_k - \vec{R}_{i\alpha}|)}{\partial q_i} \right)_{q_i=0} \\ &= \frac{1}{\sqrt{l}} \sum_\alpha \left(\frac{\partial W(|\vec{r}_k - \vec{R}_{i\alpha}|)}{\partial R_{i\alpha}} \right)_{\vec{R}_{i\alpha}=\vec{R}^0_{i\alpha}} \end{aligned} \tag{5}$$

where $\vec{R}_{i\alpha}$ are the coordinates of the ligand surrounding of the metal site i and $\vec{R}^0_{i\alpha}$ are their equilibrium values, α numbers the ligands in the first coordination sphere, l is their total number. In the exchange–charge model of the crystal field[26]

$$V_{\mathrm{c}} = \sum_{k,\alpha} W(|\vec{r}_k - R_{i\alpha}|) = \sum_{k,p,m} B_p^m C_p^m(\vartheta_k, \varphi_k) \tag{6}$$

is the crystal field potential acting on the electronic shell of the metal ion. In eqn. (6) $C_p^m(\vartheta_k,\varphi_k) = (4\pi/(2p+1))^{1/2} Y_{pm})$ are spherical operators, the parameters B_p^m are represented in the form

$$B_p^m = B_p^{m(\mathrm{pc})} + B_p^{m(\mathrm{ec})}, \tag{7}$$

here the indices pc and ec identify the partial contributions to the crystal field from the point charges of lattice ions and the exchange charges.The component $B_p^{m(\mathrm{pc})}$ is determined in the usual manner.[26] The parameter $B_p^{m(\mathrm{ls})}$ is given by the following relation:

$$B_p^{m(\mathrm{es})} = \frac{2e^2(2p+1)}{5} G_p \sum_\alpha \frac{S_p(R_\alpha)}{R_\alpha} C_p^{m^*}(\vartheta_\alpha, \varphi_\alpha) \tag{8}$$

where G_p ($p = 2,4$) are dimensionless parameters of the model obtained from a comparison of the calculated and measured crystal-field splittings of the d-levels of V^{4+} and Mo^{5+} ions,

$$S_p(R_\alpha) = (S_s(R_\alpha))^2 + (S_\sigma(R_\alpha))^2 + \gamma_p(S_\pi(R_\alpha))^2, \tag{9}$$

$\gamma_2 = 1$, $\gamma_4 = -4/3$, the overlap integrals $S_s(R_\alpha) = \langle n\mathrm{d}, m = 0|2\mathrm{s}\rangle$, $S_\sigma(R_\alpha) = \langle n\mathrm{d}, m = 0|2\mathrm{p}, m = 0\rangle$, $S_\pi(R_\alpha) = \langle n\mathrm{d}, m = 1|2\mathrm{p}, m = 1\rangle$ have been calculated using the radial 3d and 4d wave functions of the V^{4+} and Mo^{5+} and the 2s, 2p wave functions of the O^{2-} ion given in ref. 30. The symmetry of the unimpaired units MO_6 comprising the Keggin molecule was assumed to be C_{4v}, the symmetry of the ill-defined moieties $M((O_t)_{1-s_i}(O_p)_{1-y_i}(O_b)_{4-x_i}H_{\alpha z_i})$ was taken in accordance with the scheme of reduction of the C_{4v} group on the subgroups. The one-electron vibronic coupling parameters

$$v_i^\Gamma = \left\langle \varphi_{\Gamma\gamma}(\vec{r}_k) | v_i(\vec{r}_k) | \varphi_{\Gamma\gamma}(\vec{r}_k) \right\rangle, \tag{10}$$

were calculated with the aid of eqn. (4)–(8). In eqn. (10) $\varphi_{\Gamma\gamma}(\vec{r}_k)$ is the wave function of the electron occupying the orbital Γ, Γ is the irreducible representation of the point group of the $M((O_t)_{1-s_i}(O_p)_{1-y_i}(O_b)_{4-x_i}H_{\alpha z_i})$ unit, γ enumerates the basis functions of Γ.

The shape and the intensity of the IVCT bands are determined not only by the vibronic coupling parameters but also by the parameters characterizing electron transfer between different metal sites of the Keggin molecule. It is known[28] that the intensity of an IVCT transition is proportional to the square of the electron transfer parameter. Hence, the most intense charge transfer bands arise from the transitions in which, under the action of light, the only electron jumps from its original site to a neighbouring one. Therefore, while calculating the absorption spectrum of a reduced Keggin unit we only take into account single-electron transfers between adjacent edge-sharing and corner-sharing metal sites. Confining ourselves to the consideration of the IVCT transitions in the visible and near-IR range, we only allow for the transfer of the excess electron between the ground states of neighbouring metal sites. Four single transfer parameters p_1, p_2, p_3, p_4 are involved in the model. The parameters p_1 and p_2 describe single-electron transfer between neighbouring edge-sharing and corner-sharing V and Mo sites, respectively. The parameters p_3 and p_4 relate to the pair Mo–Mo. For example, the transfer parameter p_3 can be expressed as

$$p_3 = \langle \varphi_{\Gamma_{\mathrm{gr}}}(i) \mid h \mid \varphi_{\Gamma_{\mathrm{gr}}}(j) \rangle, \tag{11}$$

here $\varphi_{\Gamma gr}(i)$ and $\varphi_{\Gamma_{\mathrm{gr}}}(j)$ are the ground orbitals of the Mo^{5+} ions occupying the edge-sharing sites i and j in one of the four triads $\mathrm{M_3O_{13}}$ composing the Keggin structure. It should be mentioned that the number of the transfer parameters was reduced to four by neglecting the differences arising from the two-electron contributions.[31] Microscopic estimations testify that the transfer parameters p_1, p_2, p_3 and p_4 are small in comparison with the vibronic coupling constants $v_i^{\Gamma_{\mathrm{gr}}}$ for the ground orbitals calculated as described above, see eqn. (5)–(10). This allows us to consider the tunnel interaction as a perturbation and to identify the stationary states of the system with those in which the excess electrons are localized. Then we employ the adiabatic approximation, neglecting the nuclear kinetic energy in the Hamiltonian eqn. (3). The energies of a Keggin molecule thus obtained represent the adiabatic potentials. This approach was used in ref. 32 and 33 and was shown to give good results when calculating spectroscopic and thermodynamic characteristics of mixed-valence systems. Taking the above into account we reduce the problem of calculation of the IVCT band positions of the whole Keggin unit (intact or defective) to that of light-induced electron transfer between two adjacent metal ions (Mo^{5+}, Mo^{6+} or V^{4+}, Mo^{6+}). Besides the IVCT transitions for V^{4+} and Mo^{5+} ions the d–d transitions from the ground states to the excited ones are taken into account. The full spectrum (*i.e.* the observed spectrum) of the Keggin unit can be obtained by summation over spectra originating from all possible single-electron transfers between neighbouring corner- and edge-sharing sites and d–d transitions in Mo^{5+} and V^{4+} ions, taking into account in each case the thermal population of the initial adiabatic potential sheet participating in the optical transition. The considerations given above led us to a study of optical electron transfer and d–d bands of binuclear clusters consisting of metal ions joined through an edge or an apex and containing a single electron over the filled shells of these ions (clusters Mo^{5+}–Mo^{6+} or V^{4+}–Mo^{6+}).

Further the structure of reduced binuclear mixed-valence species responsible for the spectral transformations on different stages of the experiment will be denoted as $((\mathrm{O_t})_{1-s1}(\mathrm{O_p})_{1-y1}(\mathrm{O_b})_{3-x1}\mathrm{H}_{\alpha z1})\mathrm{d}^1\text{–}\mathrm{O_b}\text{–}\mathrm{d}^0((\mathrm{O_t})_{1-s2}(\mathrm{O_p})_{1-y2}(\mathrm{O_b})_{3-x2}\mathrm{H}\beta_{z2})$, where d^1 designates the 3d or 4d-electron, and the meaning of all other symbols remains the same as above. The composition of very likely species was chosen on the basis of the thermal gravimetric, differential thermal and IMR-MS analysis,[2,23] geometric structure of $\mathrm{MoO_3}$ and quantum-mechanical calculations of proton affinities.[34] The intervalent transitions in species $((\mathrm{O_t})_{1-s1}(\mathrm{O_p})_{1-y1}(\mathrm{O_b})_{3-x1}\ \mathrm{H}_{\alpha z1}\ )\mathrm{d}^1\text{–}\mathrm{O_b}\text{–}\mathrm{d}^0((\mathrm{O_t})_{1-s2}(\mathrm{O_p})_{1-y2}(\mathrm{O_b})_{3-x2}\mathrm{H}\beta_{z2})$ have one maximum at the point[25]

$$(\hbar\Omega)_{\max} = \frac{v_2^2}{2\hbar\omega} + \frac{\Delta}{2} + \left[\left(\frac{v_2^2}{2\hbar\omega} + \frac{\Delta}{2}\right)^2 - \frac{T(v_1^2 + v_2^2)}{2\hbar\omega}\right]^{1/2} \tag{12}$$

here ν_1 and ν_2 are the vibronic coupling constants for the moieties $\mathrm{d}^1((\mathrm{O_t})_{1-s1}\ (\mathrm{O_p})_{1-y1}(\mathrm{O_b})_{4-x1}\mathrm{H}_{\alpha z1})$ and $\mathrm{d}^1((\mathrm{O_t})_{1-s2}\ (\mathrm{O_p})_{1-y2}(\mathrm{O_b})_{4-x2}\mathrm{H}\beta_{z2})$, respectively, and Δ is the energy gap between the ground orbitals of these moieties. The calculated maxima of charge transfer bands arising from intact and some ill-defined bi-nuclear species are listed in Tables 3 and 4.

Table 3 Calculated positions of the charge-transfer (CT) and d–d bands arising from different types of species in the Vis range

Species	Band	Temperature /K	Position /nm
$(\mathrm{O_tO_p(O_b)_3)H_{b1})V^{4+}\text{–}O_b\text{–}Mo^{6+}(O_tO_p(O_b)_3)}$	CT	330	830[a]
$(\mathrm{O_tO_p(O_b)_3)V^{4+}\text{–}O_b\text{–}Mo^{6+}(O_t(O_b)_3)}$	CT	500	755
$(\mathrm{O_t(O_b)_2)Mo^{5+}\text{–}O_b\text{–}V^{5+}(O_tO_p(O_b)_3)}$	CT	500	750
$(\mathrm{O_t(O_b)_2)Mo^{5+}\text{–}O_b\text{–}Mo^{6+}(O_tO_p(O_b)_3)}$	CT	500	722
$(\mathrm{O_tO_p(O_b)_2)Mo^{5+}\text{–}O_b\text{–}Mo^{6+}(O_tO_p(O_b)_2)}$	CT	500	664
$(\mathrm{O_t\ (O_b)_2)V^{4+}\text{–}O_b\text{–}Mo^{6+}(O_tO_p(O_b)_3)}$	CT	500	600
$(\mathrm{O_tO_p(O_b)_2)Mo^{5+}\text{–}O_b\text{–}V^{5+}(O_tO_p(O_b)_3)}$	CT	500	552
$(\mathrm{O_tO_p(O_b)_2)V^{4+}\text{–}O_b\text{–}Mo^{6+}(O_tO_p(O_b)_2)}$	CT	500	543
$(\mathrm{O_tO_p(O_b)_2)Mo^{5+}\text{–}O_b\text{–}Mo^{6+}(O_tO_p(O_b)_3)}$	CT	500	537
$(\mathrm{O_tO_p(O_b)_2)V^{4+}\text{–}O_b\text{–}Mo^{6+}(O_tO_p(O_b)_3)}$	CT	500	457
$(\mathrm{O_tO_p(O_b)_4)V^{4+}}$	d–d		769, 625
$(\mathrm{O_tO_p(O_b)_4H_{b1})V^{4+}}$	d–d		743, 720, 519
$(\mathrm{O_tO_p(O_b)_4)Mo^{5+}}$	d–d		712, 444
$(\mathrm{O_tO_p(O_b)_4H_{b1})Mo^{5+}}$	d–d		701, 505, 498

[a] This band is on the border of the Vis and near-IR range in the temperature interval of crystal water loss.

Table 4 Calculated positions of the charge-transfer bands in the near-IR range

Species	Temperature/K	Band position/nm
$(\mathrm{O_tO_p(O_b)_3H_{b1})V^{4+}O_b\text{–}Mo^{6+}(O_tO_p(O_b)_3H_{b1})}$	340	922
$(\mathrm{O_tO_p(O_b)_3)V^{4+}\text{–}O_b\text{–}Mo^{6+}(O_tO_p(O_b)_3)}$	340	1012
$(\mathrm{O_tO_p(O_b)_3H_{b1})Mo^{5+}\text{–}O_b\text{–}Mo^{6+}(O_tO_p(O_b)_3)}$	340	1011
$(\mathrm{O_tO_p(O_b)_3H_{b1})Mo^{5+}\text{–}O_b\text{–}V^{5+}(O_tO_p(O_b)_3)}$	340	1068
$(\mathrm{O_tO_p(O_b)_3H_{b1})Mo^{5+}\text{–}Mo^{6+}(O_tO_p(O_b)_3H_{b1})}$	340	1142
$(\mathrm{O_tO_p(O_b)_3)Mo^{5+}\text{–}Mo^{6+}(O_tO_p(O_b)_3)}$	340	1224
$(\mathrm{O_tO_p(O_b)_3)V^{4+}\text{–}O_b\text{–}Mo^{6+}(O_p(O_b)_3)}$	560	1091
$(\mathrm{O_tO_p(O_b)_3)Mo^{5+}\text{–}O_b\text{–}V^{5+}(O_t(O_b)_3)}$	560	1000
$(\mathrm{O_p(O_b)_3)V^{4+}\text{–}O_b\text{–}Mo^{6+}(O_p(O_b)_3)}$	560	980
$(\mathrm{O_tO_p(O_b)_3)Mo^{5+}\text{–}O_b\text{–}Mo^{6+}(O_t(O_b)_3)}$	560	873

Quantum-mechanical calculations[25] show that reduced binuclear species with protons localized on the bridging oxygens (Tables 3 and 4) or with vacancies of the bridging oxygens (Table 3) give blue shifted charge transfer bands relative to those arising from intact ones; a proton on the terminal oxygen leads to a red shift. The Vis part of the spectra in heteropoly acids and Cs-salts is revealed to be formed by d–d and IVCT transitions V^{4+}–O–$Mo^{6+} \rightarrow V^{5+}$–O–$Mo^{5+}$, Mo^{5+}–O–$Mo^{6+} \rightarrow Mo^{6+}$–O–$Mo^{5+}$ (Table 3). Depending on temperature, the IVCT transitions arise from species $(O_tO_p(O_b)_3H_{b1})V^{4+}$–$O_b$–$Mo^{6+}(O_tO_p\,(O_b)_3)$with a proton localized on the bridging oxygen or reduced species of the type of $VMoO_{10}$, $VMoO_9$, Mo_2O_{10}, Mo_2O_9 with one or two oxygen vacancies[25] (Table 3).

At RT after a certain time on gas flux (for example, He (Fig. 2)) in HPA the loss of crystal water begins. At this initial stage there is no reduction, the HPA is partly in the hydrated phase, the protons are not localized and reside on the bridging water moieties $H_5O_2^+$. However, the quantitative determination of the V^{4+} content by EPR[10] shows that even at this stage vanadium is present as V^{4+}, its amount is about 0.5–2 mol%. At the same time a small amount of Mo^{5+} is also detected. Thus initially, the Vis part of the spectra originates mainly from the d–d transitions in the contained V^{4+} and Mo^{5+} ions.[28] The total spectrum intensity increases due to the increase in the intensity of the charge transfer band arising from the V^{4+}–Mo^{6+} intervalent transition in intact species $VMoO_{11}$ [28] which contributes to the first near-IR band (Table 4 and section 4.5.). At temperatures 326–422 K the removal of crystal water (see thermogravimetric (TG) data in Table 1) is accompanied by the localization of acidic protons, the most energetically favourable sites of which have been shown to be the bridging oxygens[34,35] All reduced species with protons residing on the bridging oxygens listed in Tables 3 and 4 give rise to new d–d transitions blue shifted in comparison with those arising from intact $VMoO_{11}$ clusters (Table 3). Besides this, at temperatures 326–422 K on the border of the Vis and near-IR range a new charge transfer band originating from the $(O_tO_p(O_b)_3H_{b1})V^{4+}$–$O_b$–$Mo^{6+}(O_tO_p(O_b)_3)$ species appears (Table 3). On the other hand, with temperature rise in the region of crystal water loss the concentration of reduced protonated species increases as fast as the protons localize on the oxygens of the reduced intact species. Both mentioned factors lead to the observed gradual blue shift of the Vis peak position in HPA and Cs_2A (Table 2). At the same time, the spectrum intensity increases due to increase in the transfer parameter with water loss. However, in spite of the smaller number of localized protons for Cs_2A in the region of crystal water loss, the blue shift of the Vis band is of the same order for HPA and Cs_2A. This can be explained by the stronger crystal field and electron–vibrational coupling in Cs_2A.

As the temperature continues to rise, constitutional water evolves (see TG data in Table 1). This water is formed by the extraction of an oxygen by two protons and leads to the formation of defective clusters in which bridging oxygens are removed. However, the constitutional water evolution itself is not accompanied by the appearance of new reduced clusters. Therefore, at this stage the transformations of the spectra may occur due to the reduced species of the type of $VMoO_{10}$, $VMoO_9$, Mo_2O_{10}, Mo_2O_9 enumerated in Table 3 and formed from reduced protonated species. Meanwhile, the evolution of molecular oxygen may lead to the formation of the same clusters $VMoO_{10}$, $VMoO_9$, Mo_2O_{10}, Mo_2O_9 from intact non-reduced VMo_{11}, Mo_2O_{11} ones. The indicated ill-defined species promote a further blue shift of the Vis band.Their concentration increases with temperature rise, and the total intensity of the Vis part of the spectra grows. After crystal water removal for Cs_2A the position of the Vis band remains nearly unchanged insofar as, due to the structure of this compound, the number of species with oxygen vacancies formed in the course of constitutional water release is approximately two times smaller than in HPA. The propene atmosphere leads to the same effects in the Vis part of HPA and Cs_2A spectra. However, propene is more efficient in the extraction of water than He, due to the additional reaction leading to the product isopropanol. Therefore, for propene–HPA the Vis band shift is larger, and in Cs_2A the Vis peak position stabilizes at lower temperatures.

Under action of O_2 the band in the Vis part of the HPA spectrum disappears after the crystal water loss.At the same time under O_2 flux in Cs_2A salt the Vis peak can be observed from RT to 663 K, and this is due to the presence of Cs^+ ions which prevent oxidation.

The spectroscopic changes in the UV/Vis range at the highest temperature (607 K, 663 K) are shown in Figs. 4 and 5. HPA treated in He develops a clear absorption band at 665 nm (directly observed in the spectra, deconvoluted on two bands at 660 and 740 nm, see section 3). For Cs_2A treated in He as well a broader absorption band at 715 nm (directly observed in the spectra deconvoluted on two bands at 680 nm and 770 nm, see section 3) is detected (not shown). At 663 K the Vis peak position for Cs_2A treated in He (Table 2) is close to that of HPA, permitting the conclusion that MoO_3 and Cs_3A salt are formed from Cs_2A in good agreement with a Raman shift of the main Keggin band from 988 cm^{-1} for Cs_2A to 992 cm^{-1} for Cs_3A.[13] This spectroscopic feature indicates an expulsion of vanadyl species based on the calculated peak maximum at 660/740 nm for HPA and 680/770 nm for Cs_2A. These conclusions can also be drawn on the basis of observed absorption bands of $VOSO_4{\cdot}5H_2O$ at 625 and 766 nm.[36] However, corresponding Raman bands indicating vanadyl species could not be observed for these catalysts treated in He.[13] The absorption band at 665 nm that is observed in the presence of He disappears in the presence of O_2 for HPA (Fig. 4). It also suffers a red shift and is weaker for Cs_2A treated in O_2. As for the Vis peak position in Cs_2A, it can be recognized that this position regains its RT_2 value at higher temperatures. Hence, the presence of molecular O_2 could stabilize the Cs_2A structure. In HPA, He/H_2O effects an even stronger Vis absorption band at *ca.* 665 nm than pure He. In this case the expulsion of vanadium species seems to be clearer, still in contrast to the Raman observation (no corresponding bands). For Cs_2A treated in He/H_2O a weaker Vis band, which is red shifted, could indicate a smaller number of expelled vanadyl species. HPA treated in propene shows a very broad weak absorption band with an observed peak maximum at *ca.* 635 nm and 2 deconvoluted spectra whose peak maxima are around 520 and 650 nm (not shown). In contrast, for Cs_2A treated in propene as for HPA

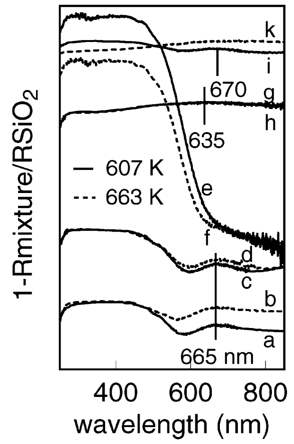

Fig. 4 Influence of gas atmospheres on the *in situ* UV/Vis spectra of $H_4PVMo_{11}O_{40}$ at 607 and 663 K. a,b: He; c,d: He/H_2O; e,f: O_2; g,h: propene; i,k: O_2/propene. For better visualization the spectra were vertically shifted.

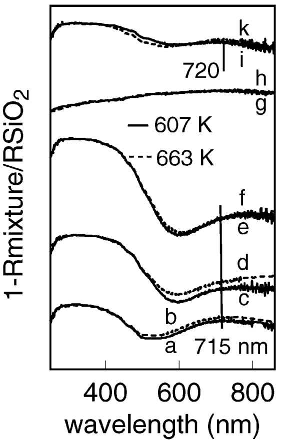

Fig. 5 Influence of gas atmospheres on the *in situ* UV/Vis spectra of $H_2Cs_2PVMo_{11}O_{40}$ at 607 and 663 K. a,b: He; c,d: He/H_2O; e,f: O_2, one of the two O_2/$H_2Cs_2PVMo_{11}O_{40}$ data sets was used; g,h: propene; i,k: O_2/propene. For a better visualization the spectra were vertically shifted.

in the presence of O_2/propene at 665 K no peak positions could be definitely detected. An observed blue shifted peak position does not exist in the presence of the mixture of O_2/propene, either for HPA or Cs_2A. At *ca.* 605 K for HPA and Cs_2A, peaks can be recognized at *ca.* 670 nm and 720 nm, respectively. However, at the highest temperature of 665 K only a very broad weak absorption band is detected for Cs_2A. This weak absorption band has a nearly symmetrical shape with the peak maxima of *ca.* 720 nm (Cs_2A) and can be fitted exactly by one Gauss curve. The bands at 670 nm (HPA, 605 K) and 720 nm (Cs_2A, 605 K, 665 K) point once again to vanadyl species. Raman spectra show bands at 1030 cm^{-1} and 1008/1002 cm^{-1} which were assigned to both vanadyl (HPA) and to molybdenyl species (HPA, Cs_2A).[13] In addition, the peak intensities of the Vis absorption band for HPA are obviously lower than that of Cs_2A indicating the lower conversion of O_2 (Figs. 4 and 5 and section 4.3.).[16] One can conclude that Cs_2A is structurally and electronically much more stable than HPA.

4.5 Influence of gas atmospheres on the near-IR peak position between RT and 663 K

The first near-IR peak position (that is the near-IR peak position with the lower wavelength in comparison with the second near-IR peak position) in the presence of He, He/H_2O or the mixture of O_2/propene shows a maximum for HPA around 512 K, as can be seen in Table 5. However, in HPA above 512 K a blue shift is detected in the presence of He, He/H_2O and the mixture of O_2/propene. A maximum at *ca.* 467 K is observed for HPA in the presence of propene and then a further increase in the peak position above 561 K. Using O_2, peak positions are only observed up to 467 K and those show a blue shift up to 422 K. Only He/H_2O shows a stabilizing effect up to *ca.* 422 K for HPA (Table 5). A decrease of the near-IR peak position is detected for Cs_2A after 467 K in the presence of He/H_2O and over the whole temperature range for the mixture of O_2/propene whereas under He, after a decrease the peak position again reaches a maximum above 467 K (Table 5). The propene near-IR peak position increases up to 608 K, and O_2 yields a broad maximum around 422 K. In this way it is confirmed that for temperatures lower than 570 K the trend in behaviour of the near-IR position for O_2/Cs_2A can be reproduced.

The second near-IR peak position has not been plotted and discussed here since it is difficult to determine definitely the position of this band due to its strong overlap with the first near-IR band.

On the basis of quantum mechanical calculations[25] it can be concluded that independent of the gas atmosphere (O_2/propene, He or He/H_2O), the main trend in the temperature behaviour of the first near-IR band of the HPA consists in the following: At RT the first near-IR band originates from the heteronuclear intervalent transitions V^{4+}–Mo^{6+}. In the range

Table 5 Near-IR peak positions of $H_4PVMo_{11}O_{40}$ and $H_2Cs_2PVMo_{11}O_{40}$ in dependence on some gas atmospheres and temperature

	Near-IR peak position/nm				
Temperature /K	He	He/H_2O	Propene	O_2	O_2/propene
$H_4PVMo_{11}O_{40}$					
RT_1	—	989	901	—	924
RT_2	—	980	—	—	976
325.9	887	992	1046	978	1025
371.3	1991	980	1014	938	1074
422.1	1053	999	1058	918	1092
466.8	1093	1051	1060	1073	1119
511.5	1137	1120	990	—	1148
561.1	1121	1119	972	—	1136
607.5	1122	1063	1044	—	1099
663.1	895	1069	1165	—	1069
$Cs_2H_2PVMo_{11}O_{40}$					
RT_1	970	990	981	970	1036
RT_2	959	990	—	966	—
325.9	967	—	1049	991	997
371.3	954	980	1022	1019	1011
422.1	947	983	1015	1029	966
466.8	969	1028	1024	1020	974
511.5	982	985	1040	992	—
561.1	984	990	1076	957	967
607.5	949	963	1084	934	952
663.1	986	953	1039	940	959

of temperatures in which crystal water is removed ($T \sim 326$–422 K) the main contribution to the near-IR band is provided by the homonuclear Mo^{5+}–Mo^{6+} and heteronuclearV^{4+}–Mo^{6+} intervalent transitions in reduced species $(O_tO_p(O_b)_3H_{b1})V^{4+}$–$O_b$–$Mo^{6+}(O_tO_p(O_b)_3H_{b1})$, $(O_t$–$O_p(O_b)_3H_{b1})$-Mo^{5+}–O_b–$Mo^{6+}(O_tO_p(O_b)_3)$, $(O_tO_p(O_b)_3H_{b1})Mo^{5+}$–$O_b$–$V^{5+}$-$(O_tO_p(O_b)_3)$, $(O_tO_p(O_b)_3H_{b1})Mo^{5+}$–$O_b$–$Mo^{6+}(O_tO_p(O_b)_3H_{b1})$ with acidic protons localized on the bridging oxygens (Table 4). In ref. 25 it was shown that among these species the latter three are the most probable ones.The maxima of the charge transfer bands arising from the species $(O_tO_p(O_b)_3H_{b1})$-Mo^{5+}–O_b–$V^{5+}(O_tO_p(O_b)_3)$, $(O_tO_p(O_b)_3H_{b1})Mo^{5+}$–$O_b$–$Mo^{6+}$ $(O_tO_p(O_b)_3H_{b1})$ are red shifted in comparison with those arising from $VMoO_{11}$ species. However, the maximum of the band originating from the species $(O_tO_p(O_b)_3H_{b1})Mo^{5+}$–$O_b$–$Mo^{6+}(O_tO_p(O_b)_3)$ is close to that of the $VMoO_{11}$ species. As a result a red shift of the near-IR band is observed in the range of crystal water loss. At the same time the increase in the transfer parameter with water loss promotes the increase in the band intensity. Then at higher temperatures, before constitutional water release and oxygen evolution, a further red shift of the maximum of the near-IR band takes place, and this is in agreement with the usual behaviour of charge transfer bands with increasing temperature.[28] Further temperature increase leads to the evolution of constitutional water and molecular oxygen. The newly appeared reduced species, for instance of the type $(O_tO_p(O_b)_3)V^{4+}$–O_b–$Mo^{6+}(O_p(O_b)_3)$, $(O_tO_p(O_b)_3)$-Mo^{5+}–O_b–$V^{5+}(O_t(O_b)_3)$, $(O_p(O_b)_3)V^{4+}$–O_b–$Mo^{6+}(O_p$–$(O_b)_3)$, $(O_tO_p(O_b)_3)Mo^{5+}$–O_b–$Mo^{6+}(O_t(O_b)_3)$ (Table 4) cause a blue shift of the near-IR band. With increasing reduction, the intensity of the near-IR band increases.

Under He the Cs_2A salt demonstrates a different behaviour from the HPA behaviour of the near-IR peak position. The maxima of the bands arising from protonated clusters are higher in energy than those in acids. This may result in a slight blue shift of the near-IR peak position in the range of 326–422 K. Then, for temperatures 422–561 K, the red shift of the band may be explained by the usual temperature dependence of the charge transfer bands. The stabilization of the peak position at higher temperatures points to the fact that in Cs salts the number of ill-defined species formed under constitutional water removal is much smaller than in acids.

4.6 Influence of gas atmospheres on the band gap energy between RT and 663 K

The band gap energy values for HPA and Cs_2A under different gas atmospheres are presented in Fig. 6 as a function of temperature. For HPA treated in He, the band gap energy decreases in the temperature range RT_1–607 K. For Cs_2A under He flow a decrease in the band gap energy is observed up to 561 K, after which it remains unchanged. HPA and Cs_2A treated in He/H_2O show quite different behaviour. For HPA after an increase in the band gap energy up to 371 K, a steep decrease in this energy is detected. For the Cs_2A salt under He/H_2O flux only a decrease in the band gap energy takes place. Both catalysts show a largely similar gap feature in pure O_2: in the range RT_1–467 K a decrease in the band gap energy is observed. At higher temperatures an increase occurs for HPA, whereas, in contrast, the band gap energy remains approximately constant for Cs_2A. For HPA and Cs_2A under the propene/O_2 atmosphere the band gap energy decreases with temperature increase up to 561 K for HPA and Cs_2A. At higher temperatures it is impossible to indicate a straight trend in temperature dependence for Cs_2A. It should also be mentioned that for both catalysts the band gap energy undergoes the maximum change under action of propene/O_2 flux. In addition, for both catalysts the band gap energies were not determined for a propene atmosphere because of the very high apparent absorption in the relevant wavelength range. For the temperature behaviour of the absorption band edge under a He stream, the following qualitative explanations may be given: Due to the peculiarities of the d electrons the conduction band formed by their orbitals can be described by the approximation of strong coupling. In this approximation the width of the conduction band is proportional to the hopping integral. With loss of water the mean distance between neighbouring units diminishes, and the overlap of their wave functions increases. This in turn leads to an increase in both the hopping integral and the width of the conduction band. In consequence, the width of the forbidden band and the absorption band edge decrease. In the case of He/H_2O flux, the following interpretation may be proposed for the thermal behaviour of the band gap energy in HPA. The increase in the optical band gap at the initial stage evidences the decrease in the width of the conduction band due to the additional external hydration of the system. It is clear that at this stage, the water of the flux prevents crystal water loss. The action of the water flux turns out to be stronger than that of He and temperature. Further temperature increase in common with a He stream suppresses the hydration of the system by flux (H_2O from flux) and facilitates the release of water. Therefore, a further decrease in band gap energy is observed for HPA. Under He/H_2O the Cs_2A salt does not show an initial increase in the optical band gap because the water coordination to Cs^+ ions is obstructive. The results obtained also show that over a wide temperature range for both catalysts under O_2 flux the "drying" effect of temperature exceeds that of O_2, which consists in oxidation of the reduced ions. At higher temperatures the number of electrons in the d band decreases appreciably due to oxidation. This promotes an apparent increase in the band gap energy in HPA. The action of propene removing the water proves to be stronger than that of oxygen. That is why the band gap energy decreases under propene/O_2 atmosphere.

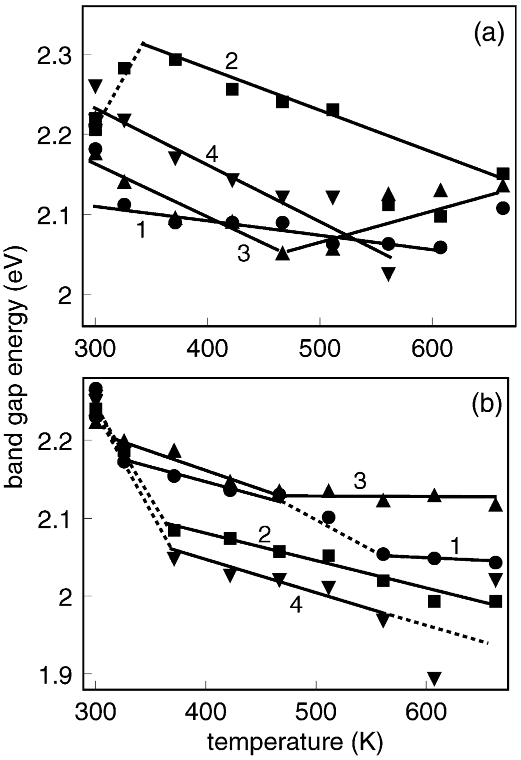

Fig. 6 Influence of gas atmospheres and temperature on the band gap energy of $H_4PVMo_{11}O_{40}$ (a) and $H_2Cs_2PVMo_{11}O_{40}$(b).1 : He; 2 : He/H_2O; 3 : O_2; 4 : O_2/ propene.

4.7 *In situ* catalytic and spectroscopic experiments of O_2/propene on HPA and Cs_2A

At 513 K on HPA a reaction and at 613 K on Cs_2A a catalytic reaction occurs with a very low product concentration of acrolein and acetic acid in the reaction gas stream. At still higher temperatures, the conversion increases and in addition to these products propanal, acetone and CO are detected.[16] Table 6 shows that the conversion of propene on HPA at 513 K and 613 K is *ca.* 3% (no conversion change) and that of O_2 *ca.* 0.3% and 2%, respectively. On Cs_2A at 613 K (first evidence of oxidation products) the conversion of propene is *ca.* 3% and that of O_2 *ca.* 12%, and the greatest selectivities were determined for acrolein and CO as may be seen in Table 7. It can be clearly recognized that for the propene oxidation on HPA the lattice oxygen is selective and the gas phase oxygen is unselective. In addition, it may be concluded from the catalytic data of the Table 6 that for HPA a catalytic reaction begins only above 573 K. The transition between the lattice and gas phase oxygen reaction cannot be recognized because a small reduction of the HPA catalyst also continues above 573 K (Table 6). For O_2/propene on Cs_2A one can determine the desired spectroscopic quantities (Vis peak position and band gap energy) only at 617 K (lowest reaction temperature). Above this temperature the low signal/noise ratio, large broadening and significant overlap of the bands prevent the determination of the mentioned spectroscopic characteristics. In contrast to the HPA investigations, gas phase oxygen appears only to be responsible for the O_2/propene reaction on Cs_2A in the temperature range of 617 to 723 K because of the much higher O_2 conversion compared to that on HPA.

5. Conclusions

Spectroscopic characteristics represented as peak intensities, peak positions and band gap energies were determined for heteropoly compounds of the type of $H_{4-x}Cs_xPVMo_{11}O_{40}$ (with $x = 0{,}2$) in the presence of different gas atmospheres over a wide range of temperatures. The obtained characteristics demonstrate an essential difference in the structural dynamics of HPA and Cs_2A under the action of different gas atmospheres. The nearly constant position of the Vis band in the range of constitutional water loss, the smaller values of the shifts of the near-IR band and sometimes opposite trends in the temperature behaviour of the band positions for Cs_2A in comparison with HPA clearly evidence that the Cs_2A compound remains stable up to higher temperatures than those for the acid. While comparing experimental data on Cs_2A and HPA with the results of quantum-mechanical calculations[25] the types of reduced dimeric V–Mo, Mo–Mo clusters contributing to the formation of the Vis and NIR bands at different temperatures were identified. With the aid of the calculated positions of the d–d and charge transfer bands originating from intact and ill-defined reduced species the behaviour of the Vis and near-IR bands in the examined compounds with increasing temperature was qualitatively interpreted. In this connection, it should be mentioned that at high temperatures ($520\ K < T < 667\ K$), especially for HPA treated in some gas atmospheres (He, He/H_2O) there is no clear trend, for example, in the temperature dependence of the Vis peak position. The following reasons can be enumerated. At high temperatures the latter cannot be singled out due to the large broadening and significant overlap of the bands. The identification of the absorption bands is also rendered more difficult because the signal/noise ratio drops with increasing temperature. If the required temperature is relatively high under stoichiometric and catalytic conditions, the broadening and overlap of the bands can also be increased by deposits and redox processes.

In the case of propene oxidation the determination of the desired quantities from the spectroscopic feature is impeded by the following circumstances: On the one hand, the reaction must be carried out at temperatures of at least 513 K for HPA and 617 K for Cs_2A in order to achieve an appreciable conversion. On the other hand, structural and electronic changes in the catalysts accompanied, for instance, by an enormous increase in the apparent absorption, already appear at low temperatures owing to the crystal water loss, which leads to the formation of isopropanol. Consequently, a correlation between the spectroscopic and analytic data could not be found. From this one can conclude that for a possible correlation between the electronic structure of the working catalyst and its performance, the optimal catalyst temperature should be $T < 623$ K for a clear observation of the spectroscopic characteristics. For this reason reactants that are not reduced too strongly by the suitable working catalysts under catalytic conditions are necessary for the investigation of the redox states.

Acknowledgement

The work was supported financially by the BMBF through its catalysis program (BMBF-Vorhaben 03D0058B). The authors are indebted to O. Timpe for preparing the heteropoly compounds and to M. Thiede for experimental assistance in UV/

Table 6 *In situ* catalytic and spectroscopic results in the propene oxidation on $H_4PVMo_{11}O_{40}$ after 1.5 h reaction time

	Conversion (%)		Selectivity (mol%)						Spectroscopic quantities	
T/*K*	Propene	O_2	Acrolein	Propanal	Acetone	CO	Acetic acid	By-product	Visible peak position /nm	Band gap energy /eV
513	3	0.3	89	—	—	—	9	2	706	2.05
573	3	0.3	40	—	—	51	8	1	692	2.0
613	3	2	34	30	6	25	4	1	679	1.96
665	12	6	24	13	6	29	26	2	—	—

Table 7 *In situ* catalytic and spectroscopic results in the propene oxidation on $H_2Cs_2PVMo_{11}O_{40}$ after 1.5 h reaction time

	Conversion (%)		Selectivity (mol%)						Spectroscopic quantities	
T/*K*	Propene	O_2	Acrolein	Propanal	Acetone	CO	Acetic acid	By-product	Visible peak position /nm	Band gap energy /eV
617	3	12	28	16	7	39	9	1	722	1.96
673	4	12	30	17	3	34	9	7	—	—
723	8	18	42	10	4	31	7	6	—	—

Vis/near-IR spectroscopy. One of the authors (S. Klokishner) is grateful to the Max-Planck-Gesellschaft for a visiting research grant.

References

1 M. Misono and N. Nojiri, *Appl. Catal.*, 1990, **64**, 1.

2 Th. Ilkenhans, B. Herzog, Th. Braun and R. Schlögl, *J. Catal.*, 1995, **153**, 275.

3 L. Weismantel, J. Stöckel and G. Emig, *Appl. Catal.*, 1996, **137**, 129.

4 B. B. Bardin and R. J. Davis, *Appl. Catal. A*, 1999, **185**, 283.

5 T. Ilkenhans, PhD. Thesis, Johann Wolfgang Goethe-Universität Frankfurt/M., 1996.

6 C. Rocchiccioli-Deltcheff and M. Fournier, *J. Chem. Soc., Faraday Trans.*, 1991, **87**(24), 3913.

7 B. W. L. Southward, J. S. Vaughan and C. T. O'Connor, *J. Catal.*, 1995, **153**, 292.

8 G. Mestl, T. K. K. Srinivasan and H. Knözinger, *Langmuir*, 1995, **11**, 3795.

9 L. Weismantel, J. Stöckel and G. Emig, *Appl. Catal.*, 1996, **137**, 129.

10 J. K. Lee, V. Russo, J. Melsheimer, K. Köhler and R. Schlögl, *Phys. Chem. Chem. Phys.*, 2000, **2**, 2977.

11 M. A. Banares, H. Hu and I. E. Wachs, *J. Catal.*, 1995, **155**, 249.

12 G. Mestl and T. K. K. Srinivasan, *Catal. Rev.-Sci. Eng.*, 1998, **40**, 451.

13 G. Mestl, T. Ilkenhans, D. Spielbauer, M. Dieterle, O. Timpe, J. Kröhnert, F. Jentoft, H. Knözinger and R. Schlögl, *Appl. Catal. A*, 2001, **210**, 13.

14 S. Berndt, PhD. Thesis, Technical University Berlin, 1998.

15 S. Berndt, D. Herein, F. Zemlin, E. Beckmann, G. Weinberg, J. Schütze, G. Mestl and R. Schlögl, *Ber. Bunsen-Ges. Phys. Chem.*, 1998, **102**, 763.

16 J. Kröhnert, Diploma Thesis, Technische Fachhochschule Berlin, 1999.

17 J. J. Altenau, M. T. Pope, R. A. Prados and H. So, *Inorg. Chem.*, 1975, **14**, 417.

18 G. Centi, J. Lopez Nieto and C. Iapalucci, *Appl. Catal.*, 1989, **46**, 197.

19 G. Centi, V. Lena, F. Trifiro, D. Ghoussoub, C. F. Aissi, M. Guelton and J. P. Bonnelle, *J. Chem. Soc., Faraday Trans.*, 1990, **86**, 2775.

20 D. Casarini, G. Centi, P. Jiru, V. Lena and Z. Tvaruzkova, *J. Catal.*, 1993, **143**, 325.

21 N. N. Timofeeva, A. V. Demidov, A. A. Davydov and I. V. Kozhevnikov, *J. Mol. Catal.*, 1993, **79**, 21.

22 J. Melsheimer, Sabri S. Mahmoud, G. Mestl and R. Schlögl, *Catal. Lett.*, 1999, **60**, 103.

23 J. K. Lee, J. Melsheimer, S. Berndt, G. Mestl, R. Schlögl and K. Köhler, *Appl. Catal. A*, 2001, **214**, 125.

24 M. Thiede and J. Melsheimer, *Rev. Sci. Instrum.*, 2002, **73**, 1.

25 S. Klokishner, J. Melsheimer, R. Ahmad, F. C. Jentoft and R. Schlögl, to be published.

26 M. N. Popova, E. P. Chukalina, B. Z. Malkin and S. K. Saikin, *Phys. Rev. B*, 2000, **61**, 7421.

27 M. Che and F. Bozon-Verduraz, in *Handbook of Heterogeneous Catalysis,* ed. G. Ertl, H. Knözinger and J. Weitkamp, Wiley-VCH, Weinheim, 1997, vol. 2, pp. 641–671.

28 S. Klokishner, J. Melsheimer, R. Ahmad, F. C. Jentoft, G. Mestl and R. Schlögl, *Spectrochim. Acta, Part A*, 2002, **58**, 1.

29 S. B. Piepho, E. R. Krausz and P. N. Schatz, *J. Am. Chem. Soc.*, 1978, **100**, 2996.

30 W. J. Pietro and W. J. Hehre, *J. Comput. Chem.*, 1983, **4**, 241.

31 J. J. Borras-Almenar, J. M. Clemente, E. Coronado and B. S. Tsukerblat, *Chem. Phys.*, 1995, **195**, 1.

32 B. S. Tsukerblat, S. I. Klokishner and B. L. Kushkuley, *Chem. Phys.*, 1992, **166**, 97.

33 S. I. Klokishner, *Chem.Phys.*, 2001, **269**, 411.

34 B. B. Bardin, S. V. Bordawekar, N. Neurock and R. J. Davis, *J. Phys. Chem.*, 1998, **102**, 10817.

35 H. Taneta, S. Katsuki, K. Eguchi, T. Seiyama and N. Yamazol, *J. Phys. Chem.*, 1986, **90**, 2959.

36 C. J. Ballhausen and H. B. Gray, *Inorg. Chem.*, 1962, **1**, 113.